

## Highly Exfoliated Nanostructure in Trifunctional Epoxy/Clay Nanocomposites Using Boron Trifluoride as Initiator

John M. Hutchinson,<sup>1</sup> Fatemeh Shiravand,<sup>1</sup> Yolanda Calventus,<sup>1</sup> Xavier Fernández-Francos,<sup>2</sup> Xavier Ramis<sup>3</sup>

<sup>1</sup>Departament de Màquines i Motors Tèrmics, Centre for NanoEngineering, ETSEIAT, Universitat Politècnica de Catalunya, 08222 Terrassa, Barcelona, Spain

<sup>2</sup>Department of Analytical and Organic Chemistry, Universitat Rovira i Virgili, C/Marcel·lí Domingo s/n, 43007 Tarragona, Spain

<sup>3</sup>Thermodynamics Laboratory, ETSEIB, Universitat Politècnica de Catalunya, 08028 Barcelona, Spain

Correspondence to: J. M. Hutchinson (E-mail: hutchinson@mmt.upc.edu)

**ABSTRACT:** Epoxy/clay nanocomposites based upon a trifunctional epoxy resin, triglycidyl p-amino phenol (TGAP), have been prepared by intercalating an initiator of cationic homopolymerization, a boron trifluoride monoethylamine (BF<sub>3</sub>·MEA) complex, into the montmorillonite clay galleries before the addition of the TGAP and the curing agent, 4,4-diamino diphenyl sulfone (DDS), and effecting the isothermal curing reaction. The BF<sub>3</sub>·MEA enhances the intragallery cationic homopolymerization reaction, which occurs before the extragallery cross-linking reaction of the TGAP with the DDS, and which hence contributes positively to the mechanism of exfoliation of the clay. The effects of isothermal cure temperature and of BF<sub>3</sub>·MEA content have been studied, in respect of both the reaction kinetics, monitored by differential scanning calorimetry, and the nanostructure, as identified by small-angle X-ray scattering and transmission electron microscopy. It is shown that the use of BF<sub>3</sub>·MEA in this way as an initiator of intragallery homopolymerization significantly improves the degree of exfoliation in the cured nanocomposites. © 2013 Wiley Periodicals, Inc. *J. Appl. Polym. Sci.* **2014**, *131*, 40020.

**KEYWORDS:** nanocomposites; montmorillonite; exfoliation; differential scanning calorimetry (DSC); epoxy resin

Received 21 June 2013; accepted 30 September 2013

DOI: 10.1002/app.40020

### INTRODUCTION

Polymer/clay nanocomposites have been intensively studied since the first disclosure of the nylon-6/montmorillonite (MMT) system by the Toyota Research Group.<sup>1–4</sup> The nanocomposites with a fine dispersion of silicate platelets in the matrix material may achieve enhanced properties, such as tensile strength and modulus,<sup>4,5</sup> barrier properties<sup>6</sup> and flame retardance,<sup>7</sup> and for use as ablative materials,<sup>8</sup> but a simple method for achieving a homogeneous distribution of randomized clay platelets in polymer matrices is still a challenging task.<sup>9–13</sup> The synthesis of nanocomposites generally occurs by one of three different methods, namely melt blending, solution blending, and *in situ* polymerization, of which the last is the relevant method when the polymer matrix is epoxy resin.

In addition to the dispersion of the clay in the epoxy matrix before curing the nanocomposite, another important factor in the overall synthesis of the nanocomposite is the polymerization reaction, and the effect on this reaction of the presence of the clay. For example, it is known that organically modified MMT clay acts as the initiator for epoxy self-polymerization,<sup>13–18</sup> and this homopolymerization reaction has been shown to be benefi-

cial in respect of the exfoliation process and the final nanostructure.<sup>13,17</sup> Consequently, it would seem appropriate to attempt to promote this homopolymerization reaction in the overall fabrication procedure for these epoxy-clay nanocomposites.

In this respect, some recent observations with a trifunctional epoxy resin, triglycidyl p-amino phenol (TGAP), are of particular interest. Multifunctional epoxy systems are of considerable interest, largely because of their high temperature capabilities, and much recent activity has been directed toward the understanding of their reaction mechanisms and kinetics under various conditions,<sup>19–24</sup> as well as studies of their rheological properties<sup>25</sup> and phase separation behavior in thermoplastic modified systems.<sup>26</sup> In particular, the trifunctional epoxy resin TGAP has been compared with resins of other functionalities (bi- and tri-) as the matrix material for polymer-layered silicate (PLS) nanocomposites,<sup>27,28</sup> and it was found, amongst other things, that the bifunctional resin gave better exfoliation than the resins of higher functionalities, and that higher cure temperatures resulted in improved clay layer separation and for some systems simultaneously increased toughness and modulus. In contrast, in our own recent work with the same TGAP resin as the matrix material for PLS nanocomposites, we have found

that better exfoliation of the clay is obtained for the TGAP system than for the equivalent system with a bifunctional epoxy, diglycidyl ether of bisphenol A (DGEBA). Specifically, in the TGAP system there appear two distinct reactions:<sup>29,30</sup> one occurs very rapidly at the start of the isothermal cure, being associated with an intragallery homopolymerization reaction triggered by the ammonium salt of the organically modified clay, while the other is associated with the bulk cross-linking process with the diamine. As it is generally considered necessary for the intragallery reaction to precede the extragallery reaction for exfoliation to occur,<sup>9,16,31–34</sup> TGAP-based PLS nanocomposites would appear to present a behavior propitious for exfoliation; what is necessary is to promote the rapid intragallery reaction in preference to the extragallery cross-linking reaction.

One possibility is to study the effect of the isothermal cure temperature,<sup>30</sup> for which it transpires that exfoliation is enhanced at higher isothermal cure temperatures, in agreement with the results of Becker et al.<sup>27,28</sup> for TGAP-based PLS nanocomposites. Another possibility is to modify the clay in such a way as to promote the intragallery homopolymerization reaction, and this is the subject of the present article. We have investigated a novel method for the fabrication of epoxy/clay nanocomposites, which is based upon the idea of increasing the rate of the intragallery reaction relative to the extragallery reaction by the addition of a suitable initiator. The initiator is a boron trifluoride monoethylamine ( $\text{BF}_3\cdot\text{MEA}$ ) complex, which is known to be an efficient initiator for the homopolymerization of epoxy resins.<sup>35–37</sup>

In the present work,  $\text{BF}_3\cdot\text{MEA}$  is first incorporated into the clay galleries before mixing the clay with the epoxy resin and curing the nanocomposite. The premise is that under these circumstances the clay layers can be more readily separated during the curing reaction by promoting the reaction within the clay galleries, which will lead to an exfoliated nanostructure in the cured nanocomposite.

## MATERIALS AND METHODS

The epoxy resin, TGAP, with trade name Araldite MY0510 (Huntsman Advanced Materials) and an epoxy equivalent between 95 and 106 g/eq, the curing agent, 4,4-diamino diphenyl sulfone (DDS), with trade name Aradur 976-1 (Aldrich), the organically modified MMT, with trade name Nanomer I.30E (Nanocor) consisting of 70–75 wt % MMT and 25–30 wt % octadecylamine, with a cation exchange capacity of 92 meq/100 g, and the  $\text{BF}_3\cdot\text{MEA}$  complex (Sigma-Aldrich) as the initiator of the cationic homopolymerization reaction, were used without further purification.

First,  $\text{BF}_3\cdot\text{MEA}$  and MMT were mixed together in various proportions (to give 0.5 wt % and 1 wt % for  $\text{BF}_3\cdot\text{MEA}$ , and 2 wt % and 5 wt % for MMT, both with respect to the TGAP content in the final nanocomposite) using acetone as a solvent, which was subsequently removed by evaporation at room temperature over a period of about 1 day. The resulting mixture, ground to a fine powder, was then dispersed in the TGAP by high shear mechanical mixing (Polytron, model PT1200C; Kinematica AG, Lucerne, Switzerland) at room temperature. This TGAP/MMT/ $\text{BF}_3\cdot\text{MEA}$  mixture was then heated on a hot plate to 80°C and the curing agent (DDS) was mixed in by hand during a period of 5–7 min to

**Table I.** The Weight Fractions (%) of Each Component in the TGAP/MMT/ $\text{BF}_3\cdot\text{MEA}$ /DDS Systems

Formulation	$\text{BF}_3\cdot\text{MEA}$	MMT	DDS	TGAP
TGAP/ $\text{BF}_3\cdot\text{MEA}$ (1.0)/DDS (52)/MMT (5)	0.6	3.2	32.9	63.3
TGAP/ $\text{BF}_3\cdot\text{MEA}$ (0.5)/DDS (52)/MMT (5)	0.3	3.2	33.0	63.5
TGAP/ $\text{BF}_3\cdot\text{MEA}$ (1.0)/DDS (52)/MMT (2)	0.6	1.3	33.6	64.5
TGAP/ $\text{BF}_3\cdot\text{MEA}$ (0.5)/DDS (52)/MMT (2)	0.3	1.3	33.7	64.7

achieve a homogeneous mixture for subsequent curing, as indicated by the mixture becoming optically clear. This mixing procedure is similar to that used by Varley et al.,<sup>19</sup> but at the lower temperature of 80°C rather than 130°C to avoid any premature crosslinking reaction of the TGAP with the DDS. According to the recommendations of the manufacturer, TGAP and DDS were used in a mass ratio of 1 : 0.52, corresponding to an average stoichiometric ratio of 1 : 0.9, assuming that the epoxy equivalent weight of the resin is in the range 95–106 g/eq.<sup>29</sup> The mixture was finally degassed under vacuum at room temperature. A summary of the various weight fractions, expressed as a percentage, of each component in the mixtures that were prepared is given in Table I.

The calorimetric experiments were carried out using a conventional differential scanning calorimeter, DSC821e (Mettler-Toledo), and a temperature modulated differential scanning calorimetry (DSC) technique, TOPEM<sup>®</sup> (DSC823e; Mettler-Toledo), both being equipped with intracooling and with STAR<sup>c</sup> software for data evaluation. Small sample quantities of the degassed resin-initiator-clay mixture (6–10 mg for DSC and 10–15 mg for TOPEM<sup>®</sup>) were placed in sealed aluminum pans and the experiments were performed under a flow of dry nitrogen gas at 50 mL/min. For this, the sealed aluminum pans were placed by robot into the DSC furnace, previously preheated to the desired isothermal cure temperature.

All the samples were cured isothermally, at one of several selected cure temperatures,  $T_c$ , with a different cure time,  $t_c$ , for each cure temperature as the reaction proceeded faster at the higher cure temperatures. In a subsequent nonisothermal scan, from 50°C to 300°C at 10°C/min in the DSC or from 100°C to 290°C at 2°C/min in TOPEM<sup>®</sup>, the residual heat of reaction and the glass transition temperature,  $T_g$ , of the fully cured nanocomposite were determined,<sup>24</sup> respectively.

A thermogravimetric analyzer (TGA, TGA/DSC 1; Mettler-Toledo) was used to determine the thermal stability and weight loss characteristics of the isothermally cured nanocomposites. The procedure was first to weigh the alumina (aluminium oxide) crucible and lid in the TGA, then the sample of mass approximately 8 mg was placed in the crucible and weighed in the TGA. Finally, the sample was heated from 40°C to 600°C at a rate of 10°C/min under a dry nitrogen gas atmosphere (200 mL/min).

The characterization of the final nanostructure of the nanocomposites was observed by transmission electron microscopy

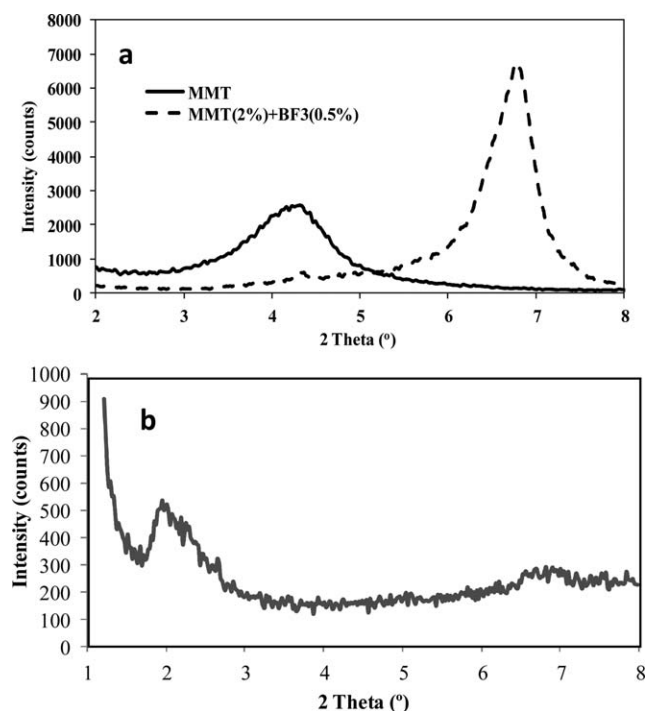


**Figure 1.** SAXS diffraction results for: (a) MMT clay (full line) and MMT/BF<sub>3</sub>·MEA mixture prepared using acetone (dashed line) and (b) MMT (2%)/BF<sub>3</sub>·MEA (0.5%) mixture after intercalation of TGAP.

(TEM), using a Jeol JeM-2010 high-resolution transmission electron microscope with a resolution of 0.18 nm at 200 kV, and by small-angle X-ray scattering (SAXS), using a Bruker D8 Advanced diffractometer, measurements being taken in a range of  $2\theta = 1\text{--}8^\circ$  with copper K $\alpha$  radiation ( $\lambda = 0.1542$  nm). For all the samples, the scans were made with steps in  $2\theta$  of  $0.02^\circ$  and with a time of 10 s for each step. Different holders were used for powder and liquid samples, so that the diffraction intensity will depend on the sample type.

## RESULTS AND DISCUSSION

### Intercalation of BF<sub>3</sub>·MEA and Epoxy Resin in MMT

The BF<sub>3</sub>·MEA and MMT were mixed in acetone with subsequent removal of the solvent. The proportions of MMT and BF<sub>3</sub>·MEA here are such that there will be either 2 wt % or 5 wt % of MMT and either 0.5 wt % or 1 wt % of BF<sub>3</sub>·MEA with respect to the TGAP amount in the final nanocomposite. This procedure is intended to intercalate the BF<sub>3</sub>·MEA into the clay galleries before adding the epoxy resin, and this was confirmed by SAXS, as shown in Figure 1(a). The  $d$ -spacing of the organically modified MMT clay alone is around 2.1 nm ( $2\theta = 4.2^\circ$ ), and when BF<sub>3</sub>·MEA is incorporated into the clay in the manner described earlier the  $d$ -spacing decreases to 1.30 nm ( $2\theta = 6.8^\circ$ ). There remains a small peak corresponding to a 2.1 nm  $d$ -spacing, implying that some of the clay layers remain with the same spacing as in the original clay, but the much stronger peak corresponding to a  $d$ -spacing of 1.3 nm can probably be attributed to the interchange of the monoethylamine of the BF<sub>3</sub> complex with the octadecyl ammonium salt of the organically modified MMT, and is therefore indicative of the presence of BF<sub>3</sub>·MEA within the clay galleries.

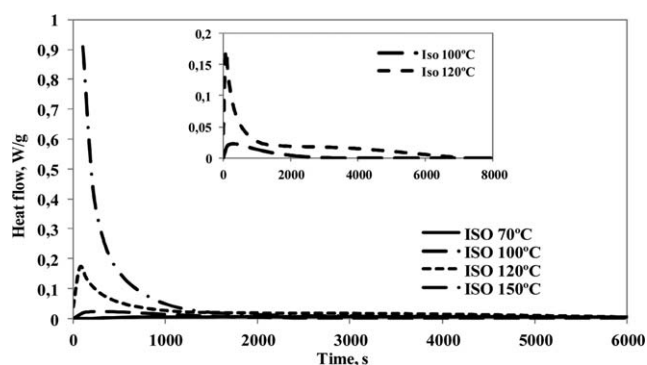


**Figure 2.** DSC scans for the isothermal cure of TGAP/DDS/MMT (5 wt %) with 1 wt % initiator (BF<sub>3</sub>·MEA) at different temperatures: 70°C (full line, almost coincident with the x-axis), 100°C (long dash), 120°C (short dash), and 150°C (dash dotted). The inset shows the first peak on an expanded scale for the samples cured at 100°C (long dash) and 120°C (short dash).

Furthermore, according to Smith et al.<sup>35</sup> and Tackie and Martin,<sup>36</sup> BF<sub>3</sub>·MEA is partially transformed into tetrafluoroboric acid HBF<sub>4</sub>, which is the initiating/catalytic species, and an amine salt at 85°C and above, and consequently it can be rationalized that BF<sub>3</sub>·MEA does not volatilize at room temperature during acetone evaporation.

When the TGAP is added to give the TGAP/MMT/BF<sub>3</sub>·MEA mixture, before the addition of the curing agent, it is anticipated that the epoxy resin will penetrate into the clay galleries, as in the TGAP/MMT system without any cationic initiator, even though the  $d$ -spacing in the clay has been reduced by the addition of the BF<sub>3</sub>·MEA complex. This is indeed confirmed by SAXS, as seen in Figure 1(b), which shows a sharp peak indicating that the resin clearly enters the clay galleries, but what is surprising is that the  $d$ -spacing increases from 1.3 nm to as much as 4.4 nm ( $2\theta = 2.0^\circ$ ). This  $d$ -spacing should be compared with that for TGAP intercalated directly into the same MMT without any BF<sub>3</sub>·MEA, which is 3.5 nm, implying a greater separation of the clay layers with the present preparation technique. Figure 1(b) also shows a small peak close to  $2\theta = 6.8^\circ$ , indicating that there remains a small proportion of clay layers with the separation of 1.3 nm, corresponding to the intercalated BF<sub>3</sub> complex.

### Kinetic Analysis

To determine the optimum cure temperature, some isothermal cure experiments were performed at different temperatures, namely 70°C, 100°C, 120°C, and 150°C, each for a cure time of 3 h, as shown in Figure 2.

In our previous work on the cure of TGAP/DDS/MMT nanocomposites,<sup>29</sup> we observed two processes occurring during isothermal curing at 150°C, the first of which could be assigned to the homopolymerization of TGAP epoxy groups initiated by the onium salt of the organomodified MMT, and the second being attributed to the epoxy-amine crosslinking reaction. In contrast, in Figure 2, only a single exothermic peak is observed for cure at 150°C. Another significant difference observed in the present study is the fact that curing in the presence of BF<sub>3</sub>·MEA proceeds

much faster than in our previous study,<sup>29</sup> from which it can be deduced that the presence of BF<sub>3</sub>·MEA has an important accelerative effect on the curing of TGAP/DDS/MMT nanocomposites.

There has been some controversy concerning the activation mechanism of the BF<sub>3</sub>·MEA complex.<sup>36</sup> On the one hand, it has been suggested by Matejka et al.<sup>38</sup> that the BF<sub>3</sub>·MEA decomposes rapidly releasing free BF<sub>3</sub>, which acts as the catalyst for the cationic epoxy homopolymerization, and releasing the amine. However, a more realistic mechanism has been proposed, by which the BF<sub>3</sub>·MEA complex is transformed into the superacid HBF<sub>4</sub>, the true catalyst.<sup>35,39</sup> Tackie and Martin<sup>36</sup> found strong evidence for the presence of the fluoroborate anion and the hydroxyl chain ends formed after initiation of the cationic homopolymerization by the proton of HBF<sub>4</sub>. Smith et al.<sup>35</sup> reported that BF<sub>3</sub>·MEA could act as a catalyst not only in tetraglycidyl diamino diphenyl methane (TGDDM) epoxy homopolymerization, but also in TGDDM-DDS epoxy-amine formulations. Moreover, they found that a similar effect could be found using a smaller amount of HBF<sub>4</sub>. They also reported that the epoxy homopolymerization was promoted by the presence of the catalyst and with a high curing temperature. The hydroxyl chain ends formed after initiation of the epoxy homopolymerization can catalyze the later reaction of TGAP epoxy groups with DDS amine groups, as is commonly accepted.<sup>40</sup> Conversely, the hydroxyl groups generated by the epoxy-amine crosslinking would not only contribute to the autocatalysis of this reaction but also contribute to accelerate further the epoxy homopolymerization as a consequence of their participation in this homopolymerization reaction by the so-called activated monomer mechanism,<sup>41</sup> as has often been reported in the cationic curing of epoxides with hydroxylic compounds.<sup>42</sup> The synergistic concurrence of both curing mechanisms could explain the strong accelerative effect observed here, in agreement with the literature.<sup>37</sup>

The fact that two processes are not observed at 150°C can be explained by the very rapid reaction and some loss of information during temperature stabilization of the DSC before the measurement starts. Figure 2 shows that, if the system is cured at 120°C, two reactions do indeed occur within the same isothermal curve: the first reaction, rather sharp, which would

correspond to the epoxy homopolymerization, the BF<sub>3</sub>·MEA complex having been activated previously during the mixing procedure at 80°C, and the second, a broad shoulder, corresponding to the epoxy-amine crosslinking. The intensity of the second process, the crosslinking reaction, decreases as the cure temperature is lowered, such that for a cure temperature of 100°C only the first process is taking place, as seen in Figure 2. For the cure at 70°C the reaction is hardly observable on the scale of Figure 2. It should be recalled that BF<sub>3</sub>·MEA must decompose to initiate the reaction, so one should assign this very small exotherm to the epoxy-amine cross-linking, although at this temperature the reaction rate is too low to be properly measured.

In previous work with TGAP/DDS/MMT, it was reported that the exfoliation of MMT could be improved by a thermal preconditioning procedure during which epoxy homopolymerization takes place inside the clay galleries.<sup>29</sup> Assuming that BF<sub>3</sub>·MEA penetrates inside the clay galleries, as deduced from the SAXS analysis results shown in the previous section, it is expected that a similar positive effect on the clay exfoliation could be achieved when BF<sub>3</sub>·MEA is used in the manner proposed here. This requires the choice of a suitable curing temperature so that, in the first place, only epoxy homopolymerization takes place, promoting the intragallery reaction, followed subsequently by postcuring at a higher temperature (or higher temperatures) to complete the crosslinking. From the results shown in Figure 2, it seems possible to separate the two reactions by choosing a temperature of 100°C. Although the inset in Figure 2 shows that the reaction is complete, and hence suggests that the sample would be cured after the first scan at 100°C in just 1 h, this is clearly not the case. For example, samples TGAP/MMT (5%)/BF<sub>3</sub>·MEA (0.5%) and TGAP/MMT (5%)/BF<sub>3</sub>·MEA (1%), both cured for 2.5 h at 100°C, have glass transition temperatures of 33.2°C and 19.1°C (in comparison with the glass transition temperature of the uncured epoxy resin of -40°C), respectively, both of these *T*<sub>g</sub>'s being much less than the isothermal cure temperature of 100°C, and even further below the *T*<sub>g</sub> of the fully cured systems (see Table II). This indicates that the sample is far from being fully cured after this

**Table II.** DSC Data From the Isothermal and Dynamic Scans of TGAP/DDS/MMT (5 wt %)/BF<sub>3</sub>·MEA (0.5 wt % or 1 wt %)

	Sample: TGAP + DDS (52%) + MMT (5%) + BF <sub>3</sub> ·MEA				
	A <sup>a</sup> (1%)	B <sup>a</sup> (1%)	C <sup>a</sup> (1%)	D <sup>a</sup> (0.5%)	E <sup>a</sup> (0.5%)
Heat of reaction, first isothermal scan (kJ/ee)	8.5	7.8	7.7	2.8	2.4
Heat of reaction, second isothermal scan (kJ/ee)	53.2	59.7	-	45.0	-
Residual heat, dynamic scan (kJ/ee)	12.8	9.1	60.5	12.9	63.3
Total heat of reaction (kJ/ee)	74.5	76.6	68.2	60.6	65.8
<i>t</i> peak, first isothermal scan (min)	6	4.1	4.8	1.9	2.0
Vitrification time, second scan <i>t</i> <sub>v</sub> (min)	47.5	18.7	-	43.4	-
<i>T</i> <sub>g</sub> for fully cured sample (°C)	246.0	249.2	245.0	247.4	246.0

An epoxy equivalent weight of 106 g/ee has been used to determine the heat of reaction in kJ/ee.

<sup>a</sup>A: isothermal cure 2.5 h at 100°C + isothermal cure 2 h at 150°C + dynamic scan 50-300°C. B: isothermal cure 2.5 h at 100°C + isothermal cure 1 h at 180°C + dynamic scan 50-300°C. C: isothermal cure 2.5 h at 100°C + dynamic scan 0-300°C. D: isothermal cure 2.5 h at 110°C + isothermal cure 2 h at 150°C + dynamic scan 50-300°C. E: isothermal cure 2.5 h at 110°C + dynamic scan 0-300°C.

curing step, and that the extent of reaction is in reality quite low, as is confirmed by the calorimetric data shown above in Table II. Moreover, it is also an indirect confirmation of the previous assumption that only the epoxy homopolymerization, not the epoxy-amine crosslinking, has taken place to a measurable extent at this temperature. It should be commented that the homopolymerization reaction has taken place not only inside the galleries but also outside, which is to be expected taking into account that the homopolymerization may start inside the galleries but propagate outside, and by the fact that not all the  $\text{BF}_3\cdot\text{MEA}$  has penetrated the clay galleries.

The same procedure was adopted for the system with 0.5 wt %  $\text{BF}_3\cdot\text{MEA}$  in TGAP/DDS/MMT (5 wt %). For this reduced proportion of  $\text{BF}_3\cdot\text{MEA}$ , the reaction at  $100^\circ\text{C}$  was slower than for the 1 wt % proportion, and for this reason a slightly higher first isothermal cure temperature of  $110^\circ\text{C}$  was selected to separate the homopolymerization and the crosslinking reactions, with a view to enhancing the intragallery reaction initiated by the  $\text{BF}_3\cdot\text{MEA}$ . Again, the first reaction was apparently complete in a cure time of approximately 1 h, but the sample showed the same signs of being only partially cured.

In fact, a cure time of 2.5 h was used in both cases to ensure as complete as possible a reaction at both  $100^\circ\text{C}$  and  $110^\circ\text{C}$ , for the formulations with 1 wt %  $\text{BF}_3\cdot\text{MEA}$  and 0.5 wt %  $\text{BF}_3\cdot\text{MEA}$ , respectively. Two temperatures were selected for the isothermal postcure of each formulation, namely  $150^\circ\text{C}$  and  $180^\circ\text{C}$  for the samples with 1 wt %  $\text{BF}_3\cdot\text{MEA}$ , and  $125^\circ\text{C}$  and  $150^\circ\text{C}$  for the samples with 0.5 wt %  $\text{BF}_3\cdot\text{MEA}$ . The postcure times were 2 h and 1 h for the temperatures of  $150^\circ\text{C}$  and  $180^\circ\text{C}$ , respectively. In this second isothermal scan (postcure), a peak in the heat flow was observed at much shorter times than for the first isothermal scan. Also during this scan, the sample vitrifies, the vitrification time,  $t_v$ , being determined by the stepwise change in  $c_{p0}$  in TOPEM. After these isothermal cure treatments, a dynamic scan was made in both DSC at  $10^\circ\text{C}/\text{min}$  and TOPEM at  $2^\circ\text{C}/\text{min}$  from  $50^\circ\text{C}$  to  $300^\circ\text{C}$  to achieve a fully cured sample and to determine its glass transition temperature,  $T_{g\infty}$ . The DSC data for the samples obtained by these various procedures are presented in Table II, and warrant some discussion, as follows.

Further evidence of the catalytic effect of  $\text{BF}_3\cdot\text{MEA}$  is seen in the vitrification time during the second isothermal scan,  $t_v$ , which here (Samples A and D in Table II, for which the second isothermal cure temperature was  $150^\circ\text{C}$ ) is about half that of the TGAP/MMT (5%)/DDS system cured isothermally at  $150^\circ\text{C}$ ,<sup>29</sup> for which vitrification times in the range between 82.7 min and 100.8 min were found, depending on whether or not the samples were first preconditioned. The catalytic effect results in a more rapid increase in the glass transition temperature as the reaction proceeds, with vitrification hence occurring earlier. For the second isothermal cure temperature of  $180^\circ\text{C}$ , vitrification occurs even earlier (Sample B, Table II), after  $<20$  min.

The heat of reaction in the first isothermal scan is significantly less for the 0.5%  $\text{BF}_3\cdot\text{MEA}$  content (Samples D and E) compared with the 1%  $\text{BF}_3\cdot\text{MEA}$  content (Samples A, B and C), indicating that the effect of the initiator is more evident for the higher  $\text{BF}_3\cdot\text{MEA}$  content. Consistent results are obtained on comparing

Samples A–C or Samples D and E. Taking a reference value of 102 kJ/ee for the curing of TGAP/DDS with 5 wt % MMT (deduced from previously published data<sup>29</sup> and assuming an epoxy equivalent weight of 106 g/ee, at the higher end of the range of values quoted by the manufacturers), it is seen that an epoxy conversion of approximately 8% can be achieved using 1 wt %  $\text{BF}_3\cdot\text{MEA}$ , which is comparable to the extent of conversion achieved by the preconditioning of TGAP with MMT at  $40^\circ\text{C}$  for 56 days.<sup>29</sup> In contrast, less than 2% conversion is achieved using 0.5 wt %  $\text{BF}_3\cdot\text{MEA}$ . Since the purpose of adding the  $\text{BF}_3\cdot\text{MEA}$  is to promote the homopolymerization reaction within the clay galleries, it is expected that a better nanostructure of the cured nanocomposites may be obtained for the higher  $\text{BF}_3\cdot\text{MEA}$  content. In practice, this does not happen, as will be shown later with the electron microscope observations of the nanostructure; a possible reason for this is that the dispersion also plays an important part in the exfoliation process. It should be commented that the reference value of 102 kJ/ee is within the range of values commonly reported, 100–110 kJ/ee, for example by Rozenberg for epoxy-amine formulations,<sup>40</sup> or by Ratna et al.<sup>43</sup> for the curing of TGAP with diethyl toluene diamine.

Some remarks should be made about the total heat of reaction obtained following the different curing schedules. In the first instance, the values reported in Table II are significantly below the reference value of 102 kJ/ee for the heat of reaction, which could be interpreted in terms of an incomplete reaction and hence a sample that is not fully cured. However, it is also seen that the glass transition temperature of the fully cured samples,  $T_{g\infty}$ , determined as the temperature at which devitrification is observed in TOPEM<sup>24</sup> during the final dynamic scan, is very similar in all cases, irrespective of the curing schedule, and only slightly lower than that of TGAP/DDS with 5 wt % MMT, namely  $251.9^\circ\text{C}$ .<sup>29</sup> In our previous work<sup>29</sup> we observed that preconditioning of the resin/clay mixture, which also results in homopolymerization of the epoxy resin, but catalyzed in this case by the onium ion of the organically modified clay, likewise leads to fully cured systems with somewhat lower values of  $T_{g\infty}$ , by as much as  $20^\circ\text{C}$  for preconditioning at the highest temperature of  $80^\circ\text{C}$ . The high values of  $T_{g\infty}$  shown in Table II indicate that a fully crosslinked network has been obtained. The slight decrease in  $T_{g\infty}$  could be explained by the plasticising effect of some unreacted DDS amine moieties as a consequence of an excessive extent of epoxy homopolymerization, which may have taken place not just inside but also outside the galleries. Therefore, the low heat of reaction observed must have a different cause.

It is usual for the total heat of reaction to be slightly less in isothermal cure compared with nonisothermal cure,<sup>34</sup> mainly as a result of some loss of the heat flow signal at the start of the isothermal experiment. The value for the heat of reaction in the second isothermal scan was determined not by a DSC experiment, as for all the other samples, but by a TOPEM experiment, which routinely results in heats of reaction slightly lower than those obtained by DSC as a consequence of the loss of a greater portion of the heat flow signal at the start of the experiment, dependent upon the width of the evaluation window used in the TOPEM analysis,<sup>44,45</sup> but this argument cannot account for such a large decrease in the total heat of reaction. Instead, we

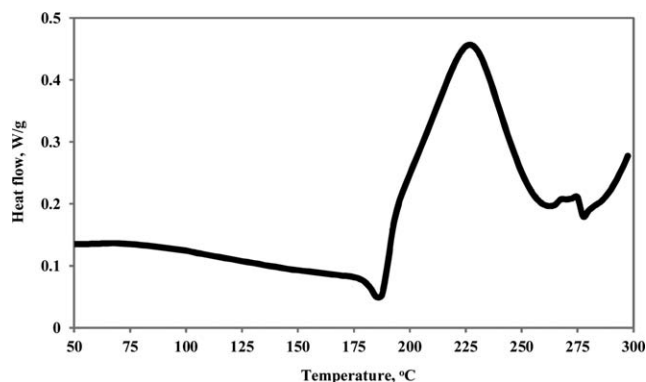


**Figure 3.** Nonisothermal DSC scan at  $10^{\circ}\text{C}/\text{min}$  for the sample TGAP/DDS/MMT (5 wt %) with 1 wt % initiator ( $\text{BF}_3\cdot\text{MEA}$ ), previously cured isothermally at  $150^{\circ}\text{C}$ . Exothermic direction is upward.

believe that it results from the effect of the beginning of the degradation process, as illustrated in Figure 3.

In this Figure, the residual exothermic reaction can be seen starting shortly after devitrification of the partially cured sample, which begins at about  $180^{\circ}\text{C}$ . The amount of residual heat of reaction is determined from the area between this curve and a baseline. However, the positioning of a baseline is subject to some uncertainty in view of the upward (exothermic) drift of the heat flow curve, which we attribute to the beginning of degradation. A similar effect was observed earlier in the nonisothermal cure of TGAP with DDS without any clay (see, for example, Figures 2 and 3 in Ref. 24), while Levchik et al.<sup>46</sup> studied the thermal degradation of DGEBA-DDM cured thermosets and found that an exothermic degradation process started at temperatures as low as  $200\text{--}250^{\circ}\text{C}$ . Because the dynamic post-curing process extends up to this temperature range, there must be an exothermic degradation reaction starting to take place at the same time. Consequently, the overlapping of the end of the curing and the beginning of degradation means that the baseline is not well defined, leading to an incorrect integration of the curing signal, and hence the low heat of reaction. The same effect applies to all the samples, especially D and E, and indeed may also explain the somewhat low heat of reaction reported in our previous work.<sup>29</sup> The thermal degradation behavior of the present samples are now discussed.

### Thermal Stability

The thermal degradation behavior of the fully cured samples was observed by TGA, and the results for Samples A, B, and D are shown in Figure 4(a). It can be seen that the major part of the degradation occurs in a single step which shows a maximum rate of weight loss at approximately  $360^{\circ}\text{C}$  for all the samples. Nevertheless, there are some noticeable differences between their behaviors. The two samples containing 1 wt %  $\text{BF}_3\cdot\text{MEA}$  but cured isothermally at either  $150^{\circ}\text{C}$  or  $180^{\circ}\text{C}$  in the second scan and then cured dynamically to  $300^{\circ}\text{C}$  (Samples A and B, respectively) show only a single step, and identical degradation behavior. On the other hand, Sample D, which contains only 0.5 wt % of  $\text{BF}_3\cdot\text{MEA}$ , shows a small step in the weight loss before the main step at  $360^{\circ}\text{C}$ . This behavior is very similar to that observed earlier<sup>18</sup> for a DGEBA epoxy resin and

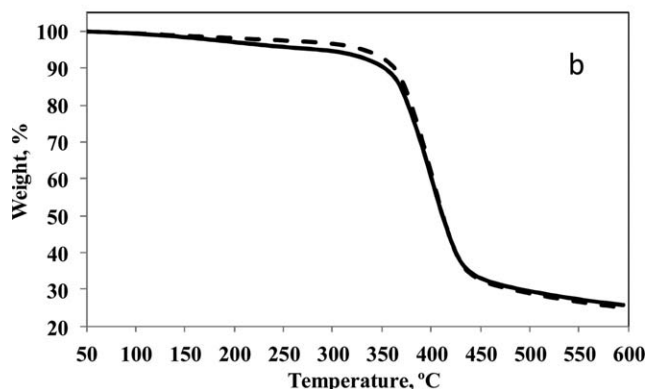
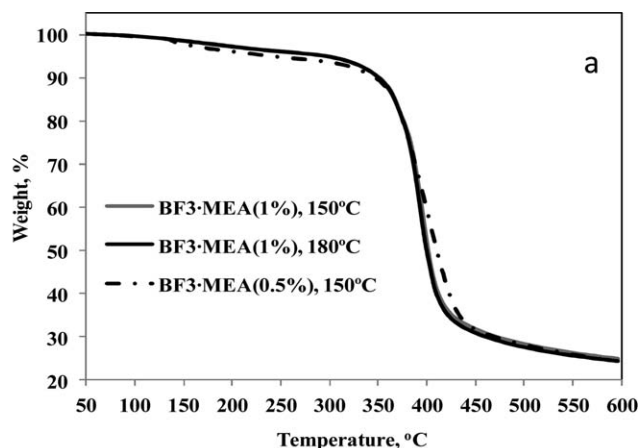


**Figure 4.** Weight percentage as a function of temperature for: (a) TGAP/MMT (5 wt %)/DDS/ $\text{BF}_3\cdot\text{MEA}$  (1, 0.5 wt %) samples after isothermal cure at the temperatures indicated, followed by a dynamic cure to  $300^{\circ}\text{C}$  and (b) TGAP/MMT/DDS/ $\text{BF}_3\cdot\text{MEA}$  (0.5 wt %) with different MMT contents: 2 wt % cured 2.5 h at  $110^{\circ}\text{C}$  + 6 h at  $125^{\circ}\text{C}$  (dashed line), and 5 wt % cured 2.5 h at  $110^{\circ}\text{C}$  + 2 h at  $150^{\circ}\text{C}$  (full line).

MMT nanocomposite system cured with a polyoxypropylene diamine, though the weight loss here is smaller and occurs at the rather lower temperature of about  $150^{\circ}\text{C}$  compared with the DGEBA system. For the mixtures of DGEBA and MMT alone, without any diamine, the TGA showed a small weight loss of up to 5% which initiated at around  $220^{\circ}\text{C}$  but which subsequently stabilized on further heating, and which was not present in the fully cured resin/clay/diamine system. This stabilization of the resin/clay mixture was attributed to the homopolymerization of the epoxy resin, catalyzed by the organically modified clay. We believe that a similar effect is happening here in Sample D, in which some unreacted moieties begin to degrade but are stabilized by a homopolymerization reaction.

Further evidence for this is presented in Figure 4(b), where the effect of decreasing the clay content to 2 wt % is shown. Here it can be seen that the small weight loss at around  $150^{\circ}\text{C}$  occurs only in the sample with 5 wt % MMT, and is absent in the sample with 2 wt % MMT. The agglomerations which form in the sample with higher clay content inhibit the complete cross-linking reaction of the intercalated epoxy resin. In fact, there is also a small displacement to higher temperature of the TGA curve in the main weight loss region for the samples with 0.5%

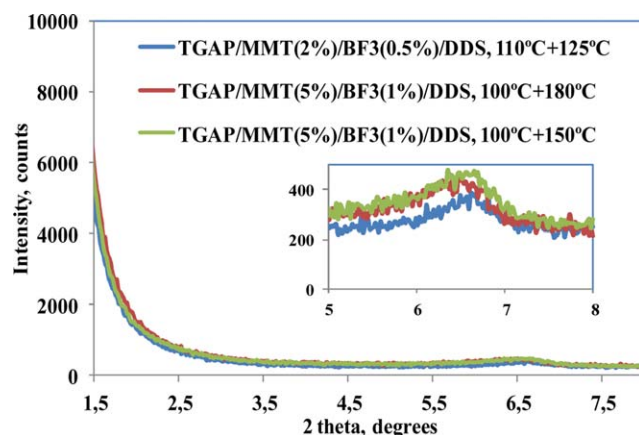


**Figure 5.** SAXS diffractograms for samples with  $\text{BF}_3$ -MEA initiator, cured and postcured at the temperatures indicated. The inset shows an enlargement of the small peak at about  $6.6^\circ$ . [Color figure can be viewed in the online issue, which is available at [wileyonlinelibrary.com](http://wileyonlinelibrary.com).]

$\text{BF}_3$ -MEA, including Sample D, again consistent with our earlier observations for the DGEBA/MMT system,<sup>18</sup> where the resin/clay system alone, without any diamine, showed a main degradation step at a somewhat higher temperature than the resin/clay/diamine system, which was attributed to the greater thermal stability of the homopolymerized nanocomposite.

#### Nanocomposite Structure

The results of the X-ray diffraction for the cured nanocomposite samples are shown in Figure 5. The absence of diffraction peaks in the low-angle region suggests that these samples are exfoliated, whether the clay content be 2 wt % or 5 wt % and also for both contents of  $\text{BF}_3$ -MEA. However, for all these samples there is a small diffraction peak, shown on an enlarged scale in the inset, close to  $2\theta = 6.6^\circ$  and corresponding to a  $d$ -spacing of 1.3 nm. This is the same  $d$ -spacing that was found for the MMT clay and  $\text{BF}_3$ -MEA preparation in which the  $\text{BF}_3$ -MEA is intercalated into the clay galleries, before the addition of the epoxy resin, as shown earlier in Figure 1. This implies that,

although the bulk of the nanocomposite appears to be exfoliated, there remains some layer stacking with a very small  $d$ -spacing within the clay agglomerations. This is indeed observed by TEM, as will be shown below.

In respect of producing an exfoliated nanostructure in the nanocomposite cured with DDS, the epoxy monomers must first be able to penetrate into the clay galleries, where either a homopolymerization reaction or a cross-linking reaction with the curing agent can be catalyzed by the surface ionic sites of the MMT. However, some extragallery cross-linking reaction will also take place at the same time, the effect of which is to inhibit the separation of the clay layers with the result that in the fully cured nanocomposite they are not generally either well separated or homogeneously distributed throughout the polymer matrix. To improve this dispersion of separated clay layers in the cured nanocomposite it is necessary to accelerate the intragallery reaction relative to the extragallery reaction, and this is achieved here by the incorporation of  $\text{BF}_3$ -MEA into the clay. From the thermal analysis results we see that the homopolymerization and the crosslinking are disassociated from each other by choosing the isothermal cure temperature correctly. Although some homopolymerization must have taken place outside the galleries, it is supposed that intragallery homopolymerization has taken place to some extent and that it will have a beneficial effect on the clay exfoliation.

From the TEM pictures of the samples with and without the  $\text{BF}_3$ -MEA initiator, it is found that the number and average size of agglomerations which are dispersed throughout the bulk of the sample are decreased significantly with the incorporation of the  $\text{BF}_3$ -MEA, as is shown in Figure 6. The micrographs shown here are representative of the whole samples and are made at the lowest magnification used, for which almost one whole grid of the TEM support is visible. Within the particular field of vision selected here, only a single agglomeration can be seen in Figure 6(a) for the sample with initiator, whereas several agglomerations of dimensions around  $10 \mu\text{m}$  can be seen in Figure 6(b) for the sample without initiator (even though this

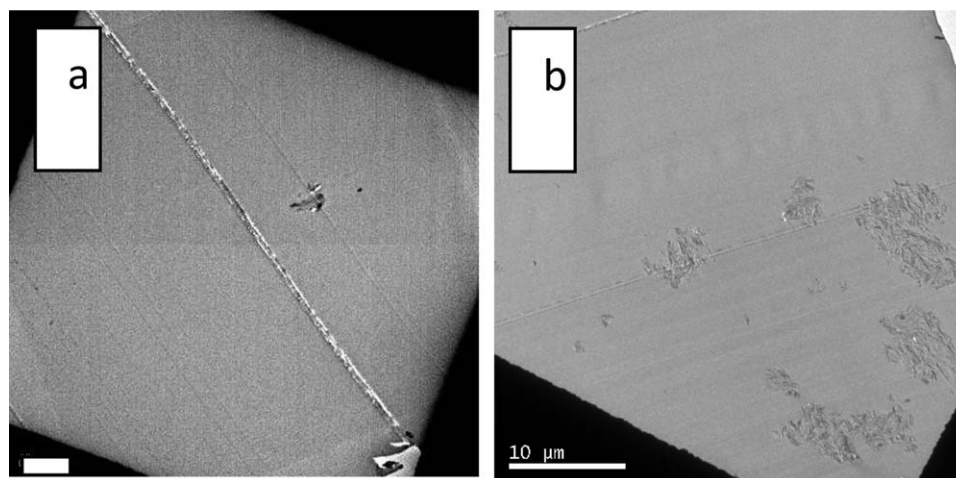


**Figure 6.** Comparison of transmission electron micrographs at low magnification for samples containing 2 wt % MMT, with and without  $\text{BF}_3$ -MEA initiator (0.5 wt %): (a) sample with 0.5 wt % initiator, cured at  $125^\circ\text{C}$  and (b) sample without initiator, cured at  $150^\circ\text{C}$  after preconditioning the TGAP/MMT mixture for 12 days at  $80^\circ\text{C}$ . Scale bar is  $10 \mu\text{m}$  in each figure.

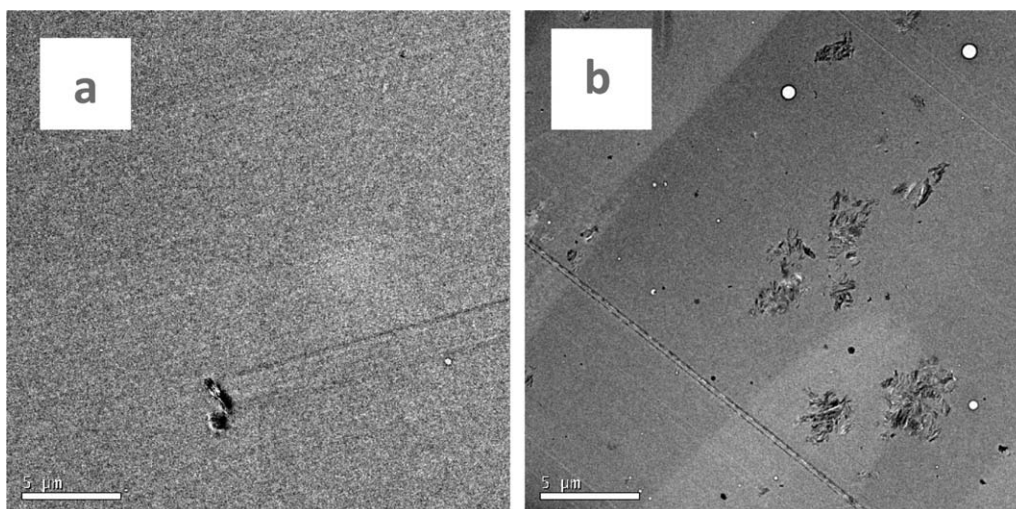


**Figure 7.** Comparison of transmission electron micrographs for samples containing 5 wt % MMT, with and without  $\text{BF}_3\cdot\text{MEA}$  initiator (1 wt %): (a) sample with initiator, cured at  $100^\circ\text{C}$  for 2.5 h and then postcured at  $150^\circ\text{C}$  for 2 h and (b) sample without initiator, cured at  $180^\circ\text{C}$  for 1.5 h. Scale bar is  $5\ \mu\text{m}$  in each figure.

sample has been preconditioned for 12 days at  $80^\circ\text{C}$ , which has improved the dispersion of the clay relative to a sample not preconditioned<sup>13,29</sup>).

At slightly higher magnification, in other samples, now with 5 wt % MMT, the same observation can be made, as shown in the transmission electron micrographs of Figure 7, which again can be considered to be representative of the whole sample. In the region shown in Figure 7(a), the sample with initiator contains a single small agglomeration, of maximum dimensions about  $2\ \mu\text{m}$ , whereas the region shown in Figure 7(b) shows a considerably larger number of agglomerations for the sample without initiator, these agglomerations also being rather larger, with maximum dimensions in the range of  $4\text{--}5\ \mu\text{m}$ . On the other hand, the single agglomeration of Figure 7(a) appears much denser than those of Figure 7(b), and this is confirmed at higher magnification.

The same single agglomeration as in Figure 7(a) is shown at higher magnification in Figure 8. Here it can be seen that within the agglomeration there remain layer stacks with a very small  $d$ -spacing. For the particular stack seen here, this spacing is about 1.3 nm, which corresponds to both that detected by SAXS for these cured nanocomposites, as seen earlier in Figure 5, as well as that for the MMT intercalated with the  $\text{BF}_3\cdot\text{MEA}$  initiator, as shown earlier in Figure 1.

It is clear from the above discussion that the incorporation of the  $\text{BF}_3\cdot\text{MEA}$  initiator improves significantly the nanostructure as identified by TEM. It remains to examine the effects of the  $\text{BF}_3\cdot\text{MEA}$  content and of the first and second isothermal cure temperatures on the agglomeration size and dispersion. First, we compare the 0.5 wt % and 1 wt %  $\text{BF}_3\cdot\text{MEA}$  contents in samples with 5 wt % MMT cured isothermally first at  $100^\circ\text{C}$  and then postcured at  $150^\circ\text{C}$ , typical transmission electron micrographs being shown in Figure 9(a,b), respectively. There appears to be no significant or systematic effect of the

$\text{BF}_3\cdot\text{MEA}$  content on the nanostructure. This is contrary to what we anticipated earlier in the discussion of the kinetic analysis and the results presented in Table II, where the DSC data showed that a greater degree of epoxy conversion could be achieved with the 1%  $\text{BF}_3\cdot\text{MEA}$  content in comparison with the 0.5% content. It seems, from observations over many regions of these ultramicrotomed sections, that samples with 1%  $\text{BF}_3\cdot\text{MEA}$  tend to display more clay agglomerations, and of a slightly larger size, though the TEM evidence is not compelling. A better comparison would be to determine a bulk property, such as the impact energy, which is also sensitive to details of the nanostructure; these experiments are currently in progress.



**Figure 8.** Agglomeration of Figure 7(a) for sample with  $\text{BF}_3\cdot\text{MEA}$  initiator, cured at  $100^\circ\text{C}$  for 2.5 h and postcured at  $180^\circ\text{C}$  for 1 h, viewed at higher magnification. Scale bar is 20 nm.

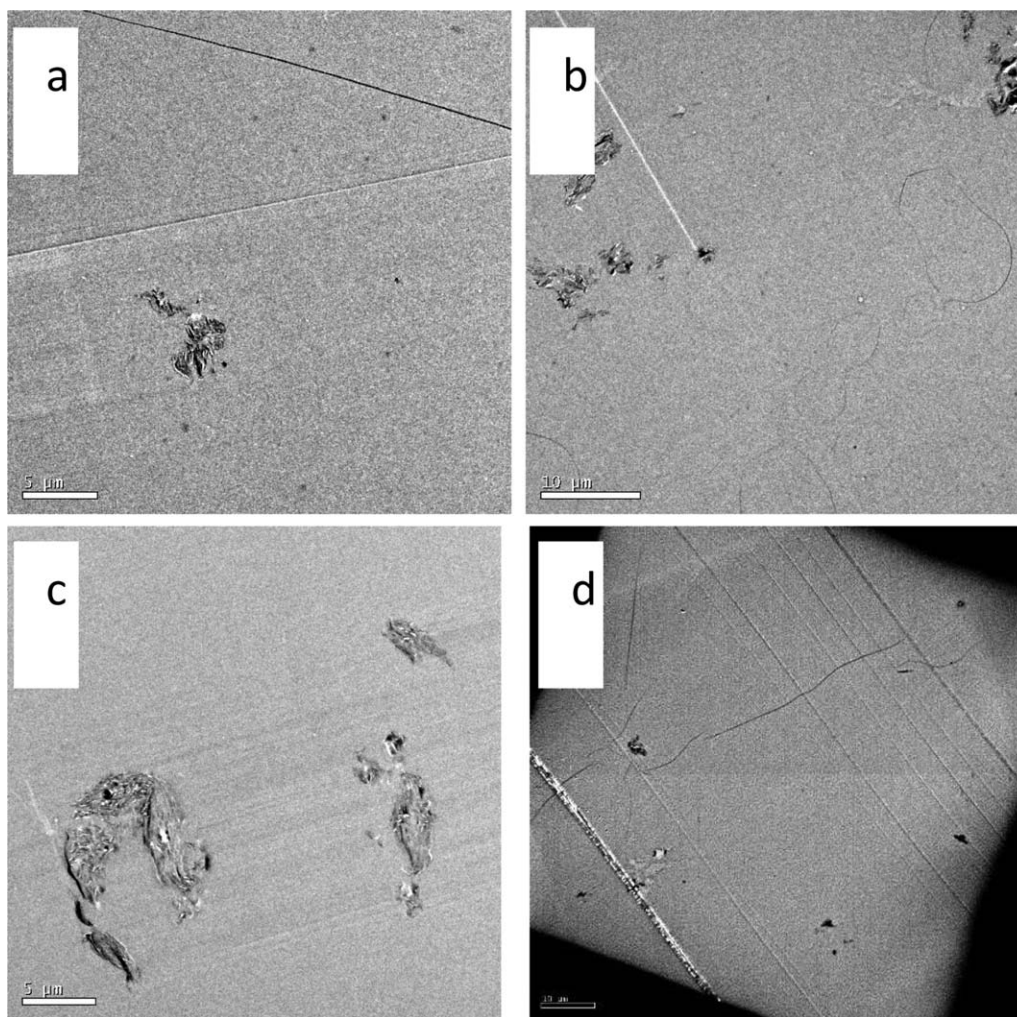


**Figure 9.** Transmission electron micrographs for TGAP/MMT/DDS/BF<sub>3</sub>·MEA nanocomposites prepared in different ways: (a) TGAP/MMT (5%)/DDS/BF<sub>3</sub> (0.5%), 100°C + 150°C (scale bar 5 μm); (b) TGAP/MMT (5%)/DDS/BF<sub>3</sub> (1%), 100°C + 150°C (scale bar 10 μm); (c) TGAP/MMT (5%)/DDS/BF<sub>3</sub> (1%), 100°C + 180°C (scale bar 5 μm); and (d) TGAP/MMT (2%)/DDS/BF<sub>3</sub> (0.5%), 110°C + 125°C (scale bar 10 μm).

Second, we compare the effect of the second isothermal postcure temperature for samples containing 5 wt % MMT and 1% BF<sub>3</sub>·MEA, typical transmission electron micrographs being shown in Figure 9(b,c) for the postcure temperatures of 150°C and 180°C, respectively. Again, though, no significant or systematic effect on the nanostructure can be observed, in this case for the second postcure temperature. In the same way as for the comparison of the effect of the BF<sub>3</sub>·MEA content, shown in Figure 9(a,b), when many TEM images such as those in Figure 9(b,c) were observed, the clay agglomerations were often found to be larger for the higher postcure temperature of 180°C, suggesting that the higher postcure temperature could result in smaller agglomerations, but this was not always the case. Once again, the effect on a bulk property such as the impact energy would possibly be more informative in this respect.

On the other hand, reducing the clay content to 2 wt % does result in a significantly better dispersion of the clay, as shown in Figure 9(d). This nanocomposite, with 0.5% BF<sub>3</sub>·MEA and cured first at 110°C and postcured at 125°C, displays very few clay agglomerations, which are all of a much smaller size than those

in Figure 9(a–c). The results of the same impact energy tests, to be described in a subsequent article shortly, should confirm the highly efficient reinforcement afforded by this nanostructure.

## CONCLUSIONS

The incorporation of an initiator of cationic homopolymerization, BF<sub>3</sub>·MEA, into the galleries of organically modified clay before the intercalation of a trifunctional epoxy resin, TGAP, into the same galleries facilitates the exfoliation of the clay layers in the cured nanocomposite. This effect results from the curing taking place in two competitive processes: (a) the intragallery homopolymerization of the epoxy resin and (b) the epoxy-amine extragallery condensation reaction. Epoxy homopolymerization also occurs to a lesser extent in the regions near to the external surfaces of the clay layers. The prime importance of the incorporation of the BF<sub>3</sub>·MEA in the clay before the addition of the TGAP is that it promotes the intragallery reaction, which occurs before the extragallery crosslinking reaction, thus permitting a significant improvement in the exfoliation process, and hence also in the nanostructure of the cured

nanocomposite. The effects of the preparation conditions on the final nanostructure formed have been studied. It transpires that, although the calorimetric studies suggest that a higher BF<sub>3</sub>·MEA content would lead to a greater degree of exfoliation, the TEM studies show no significant or systematic effect of BF<sub>3</sub>·MEA content. Likewise, the TEM studies also show no significant effect of the cure schedule on the nanostructure. On the other hand, samples prepared with a lower clay content do display a significantly greater degree of exfoliation.

#### ACKNOWLEDGMENTS

The authors are grateful to Huntsman Corporation for the epoxy resin and curing agent. This work was supported financially by MINECO Project MAT2011-27039-C03 and the Generalitat de Catalunya (2009-SGR-1512). FS is grateful for a grant from the Agència de Gestió d'Ajuts Universitaris i de Recerca (AGAUR), FI-DGR 2011 and XF-F acknowledges the contract JCI-2010-06187.

#### REFERENCES

1. Kojima, Y.; Usuki, A.; Kawasumi, M.; Okada, A.; Kurauchi, T.; Kamigaito, O. *J. Polym. Sci. Part A: Polym. Chem.* **1993**, *31*, 983.
2. Usuki, A.; Kawasumi, M.; Kojima, Y.; Okada, A.; Kurauchi, T.; Kamigaito, O. *J. Mater. Res.* **1993**, *8*, 1174.
3. Usuki, A.; Kojima, Y.; Kawasumi, M.; Okada, A.; Fukushima, Y.; Kurauchi, T.; Kamigaito, O. *J. Mater. Res.* **1993**, *8*, 1179.
4. Kojima, Y.; Usuki, A.; Kawasumi, M.; Okada, A.; Fukushima, Y.; Kurauchi, T.; Kamigaito, O. *J. Mater. Res.* **1993**, *8*, 1185.
5. Okada, A.; Usuki, A. *Mater. Sci. Eng. C* **1995**, *3*, 109.
6. Yano, K.; Usuki, A.; Okada, A.; Kurauchi, T.; Kamigaito, O. *J. Polym. Sci. Part A: Polym. Chem.* **1993**, *31*, 2493.
7. Lepoittevin, B.; Devalckenaere, M.; Pantoustier, N.; Alexandre, M.; Kubies, D.; Calberg, C.; Jerome, R.; Dubois, P. *Polymer* **2002**, *43*, 4017.
8. Vaia, R. A.; Price, G.; Ruth, P. N.; Nguyen, H. T.; Lichtenhan, J. *Appl. Clay Sci.* **1999**, *15*, 67.
9. Park, J. H.; Jana, S. C. *Macromolecules* **2003**, *36*, 2758.
10. Park, J. H.; Jana, S. C. *Polymer* **2003**, *44*, 2091.
11. Kong, D.; Park, C. E. *Chem. Mater.* **2003**, *15*, 419.
12. Wang, K.; Chen, L.; Wu, J.; Toh, M. L.; He, C.; Yee, A. F. *Macromolecules* **2005**, *38*, 788.
13. Pustkova, P.; Hutchinson, J. M.; Román, F.; Montserrat, S. *J. Appl. Polym. Sci.* **2009**, *114*, 1040.
14. Wang, M. S.; Pinnavaia, T. J. *Chem. Mater.* **1994**, *6*, 468.
15. Lan, T.; Kaviratna, D.; Pinnavaia, T. J. *J. Phys. Chem. Sol.* **1996**, *57*, 1005.
16. Chin, I.-J.; Thurn-Albrecht, T.; Kim, H.-C.; Russell, T. P.; Wang, J. *Polymer* **2001**, *42*, 5947.
17. Benson Tolle, T.; Anderson, D. P. *J. Appl. Polym. Sci.* **2004**, *91*, 89.
18. Hutchinson, J. M.; Montserrat, S.; Román, F.; Cortés, P.; Campos, L. *J. Appl. Polym. Sci.* **2006**, *102*, 3751.
19. Varley, R. J.; Hodgkin, J. H.; Hawthorne, D. G.; Simon, G. P. *J. Appl. Polym. Sci.* **1996**, *60*, 2251.
20. Bonnaud, L.; Pascault, J. P.; Sautereau, H. *Eur. Polym. J.* **2000**, *36*, 1313.
21. Liu, H.; Uhlherr, A.; Varley, R. J.; Bannister, M. K. *J. Polym. Sci. Part A: Polym. Chem.* **2004**, *42*, 3143.
22. Varley, R. J.; Liu, W.; Simon, G. P. *J. Appl. Polym. Sci.* **2006**, *99*, 3288.
23. Frigione, M.; Calò, E. *J. Appl. Polym. Sci.* **2008**, *107*, 1744.
24. Hutchinson, J. M.; Shiravand, F.; Calventus, Y.; Fraga, I. *Thermochim. Acta* **2012**, *529*, 14.
25. Corcione, C. E.; Frigione, M. *Polym. Test.* **2009**, *28*, 830.
26. Zhang, J.; Guo, Q.; Fox, B. L. *Compos. Sci. Technol.* **2009**, *69*, 1172.
27. Becker, O.; Cheng, Y.-B.; Varley, R. J.; Simon, G. P. *Macromolecules* **2003**, *36*, 1616.
28. Becker, O.; Simon, G. P.; Varley, R. J.; Halley, P. J. *Polym. Eng. Sci.* **2003**, *43*, 850.
29. Hutchinson, J. M.; Shiravand, F.; Calventus, Y. *J. Appl. Polym. Sci.* **2013**, *128*, 2961.
30. Hutchinson, J. M.; Shiravand, F.; Calventus, Y. *Polym. Eng. Sci.* **2013**. DOI:10.1002/pen.23540.
31. Lan, T.; Kaviratna, D.; Pinnavaia, T. J. *Chem. Mater.* **1995**, *7*, 2144.
32. Kornmann, X.; Lindberg, H.; Berglund, L. A. *Polymer* **2001**, *42*, 4493.
33. Chen, C.; Curliss, D. *J. Appl. Polym. Sci.* **2003**, *90*, 2276.
34. Montserrat, S.; Román, F.; Hutchinson, J. M.; Campos, L. *J. Appl. Polym. Sci.* **2008**, *108*, 923.
35. Smith, R.E.; Larsen, F.N.; Long, C.L. *J. Appl. Polym. Sci.* **1984**, *29*, 3713.
36. Tackie, M.; Martin, G. C. *J. Appl. Polym. Sci.* **1993**, *48*, 793.
37. Matejka, L.; Chabanne, P.; Tighzert, L.; Pascault, J. P. *J. Polym. Sci. Part A: Polym. Chem.* **1994**, *32*, 1447.
38. Matejka, L.; Dusek, K.; Chabanne, P.; Pascault, J.P. *J. Polym. Sci. Part A: Polym. Chem.* **1997**, *35*, 651.
39. Smith, R. E.; Larsen, F. N.; Long, C. L. *J. Appl. Polym. Sci.* **1984**, *29*, 3697.
40. Rozenberg, B. A. *Adv. Polym. Sci.* **1986**, *75*, 113.
41. Kubisa, P.; Penczek, S. *Prog. Polym. Sci.* **1999**, *24*, 1409.
42. Sangermano, M.; Malucelli, G.; Bongiovanni, R.; Priola, A.; Harden, A. *Polym. Int.* **2005**, *54*, 917.
43. Ratna, D.; Varley, R.; Simon, G. P. *J. Appl. Polym. Sci.* **2003**, *89*, 2339.
44. Fraga, I.; Montserrat, S.; Hutchinson, J. M. *J. Therm. Anal. Cal.* **2007**, *87*, 119.
45. Fraga, I.; Montserrat, S.; Hutchinson, J. M. *J. Therm. Anal. Cal.* **2008**, *91*, 687.
46. Levchik, S. V.; Camino, G.; Luda, M. P.; Costa, L.; Muller, G.; Costes, B. *Polym. Degrad. Stab.* **1998**, *60*, 169.